Cell, Vol. 103, 931–943, December 8, 2000, Copyright ©2000 by Cell Press

Crystal Structure and Functional Analysis of Ras Binding to Its Effector Phosphoinositide 3-Kinase γ

Michael E. Pacold,* Sabine Suire,† Olga Perisic,* Samuel Lara-Gonzalez,* Colin T. Davis,* Edward H. Walker,* Phillip T. Hawkins,† Len Stephens,† John F. Eccleston,‡ and Roger L. Williams*§
*MRC Laboratory of Molecular Biology
Hills Road
Cambridge CB2 2QH
United Kingdom
†The Babraham Institute
Babraham
Cambridge CB2 4AT
United Kingdom
‡National Institute for Medical Research
The Ridgeway
Mill Hill
London NW7 1AA
United Kingdom

Summary

Ras activation of phosphoinositide 3-kinase (PI3K) is important for survival of transformed cells. We find that PI3Kγ is strongly and directly activated by H-Ras G12V in vivo or by GTPγS-loaded H-Ras in vitro. We have determined a crystal structure of a PI3Kγ/Ras·GMPPNP complex. A critical loop in the Ras binding domain positions Ras so that it uses its switch I and switch II regions to bind PI3Kγ. Mutagenesis shows that interactions with both regions are essential for binding PI3Kγ. Ras also forms a direct contact with the PI3Kγ catalytic domain. These unique Ras/PI3Kγ interactions are likely to be shared by PI3Kα. The complex with Ras shows a change in the PI3K conformation that may represent an allosteric component of Ras activation.

Introduction

The phosphoinositide 3-kinases are a family of ubiquitous multidomain signaling proteins that phosphorylate the 3-hydroxyl of phosphoinositides. Mammalian PI3Ks are divided into three classes based on their structure and substrate specificity (Domin and Waterfield, 1997). Class I enzymes are acutely activated by a variety of cell-surface receptors, and are responsible for synthesis of intracellular phosphatidylinositol (3,4,5)-trisphosphate (PtdIns(3,4,5)P_3). Thus, stimulation of many cells results in the PI3K-dependent accumulation of PtdIns(3,4,5)P_3 in the inner leaflet of the plasma membrane. This usually transient production of PtdIns(3,4,5)P_3 initiates a multitude of further downstream signals by causing membrane recruitment of proteins that specifically bind PtdIns (3,4,5)P_3. Typically, this results in a colocalization of enzymes and substrates that fires further signaling activity. Cellular processes in which PI3Ks are essential include suppression of apoptosis (Franke et al., 1997), reorganization of the actin cytoskeleton (Rodriguez-Viciana et al., 1997), cardiac myocyte growth (Shioi et al., 2000), glycogen synthase stimulation by insulin (reviewed in Shepherd et al., 1998), TNFα-mediated neutrophil priming and superoxide generation (Condliffe et al., 1998), and leukocyte migration and adhesion to endothelial cells (reviewed in Wymann et al., 2000).

There are two types of class I PI3Ks. Class IA consists of p110α, β, and δ catalytic subunits that associate with an SH2 domain–containing subunit (p85α and splice variants of it, p85β or p55γ) that is indispensable for activation by phosphotyrosine-containing proteins (Carpenter et al., 1993). Consequently, the class IA PI3Ks are typically activated by receptors that regulate tyrosine kinases. Class IB contains only one member, PI3Kγ. This enzyme is regulated by G protein–coupled receptors via association with βγ subunits of heterotrimeric G proteins (Stoyanov et al., 1995). A p101 regulatory subunit that tightly binds p110γ is critical for Gβγ-activated PtdIns(3,4,5)P_3 production (Stephens et al., 1997; Krugmann et al., 1999; Maier et al., 1999). All class I PI3Ks have a domain that is similar to a Ras binding domain (RBD) present in other proteins that are regulated by the GTPase Ras. Furthermore, all class I PI3Ks bind Ras in a GTP-dependent manner (Rodriguez-Viciana et al., 1994; Rubio et al., 1997; Vanhaesebroeck et al., 1997; Deora et al., 1998).

The Ras family of membrane-localized GTPases transduces a variety of signals in eukaryotic cells (Lowy and Willumsen, 1993; Shields et al., 2000). The exchange of GDP for GTP causes two regions of Ras, known as switch I (residues 32–40) and switch II (residues 60–76), to change conformation (Pai et al., 1989; Milburn et al., 1990). This GTP-induced conformational change allows Ras to bind and activate multiple downstream effectors, which can cooperate to produce the diverse phenotypes characteristic of Ras transformation (White et al., 1995; Marshall, 1996) or function independently in activating survival pathways (Xue et al., 2000). Most Ras-dependent signaling is mediated by three downstream effectors: the protein kinase Raf, the exchange factor RalGDS, and PI3K (reviewed in Wittinghofer and Herrmann, 1995; Feig et al., 1996; Rodriguez-Viciana et al., 1996a).

Although all class I PI3Ks bind Ras, only PI3Kα has been shown to be directly stimulated by Ras·GTP (Rodriguez-Viciana et al., 1994, 1996b). Ras-induced activation is synergistic with p85-mediated stimulation of PI3Kα by phosphotyrosine peptides. Direct Ras activation of PI3Kα stimulates actin rearrangement and inhibits programmed cell death upon detachment from the extracellular matrix (anoikis) (Khwaja et al., 1997; Rodriguez-Viciana et al., 1997). Other consequences of Ras activation of PI3Ks include cell transformation (Gire et al., 2000), T cell adhesion and migration (Tanaka et al., 1999), and blocking of apoptosis induced by c-Myc (Kauffmann-Zeh et al., 1997) or by NGF deprivation (Xue et al., 2000).

A recent crystal structure of PI3Kγ (Walker et al., 1999) showed that the Ras binding domain of the kinase packs

§To whom correspondence should be addressed (e-mail: rlw@mrc-lmb.cam.ac.uk).

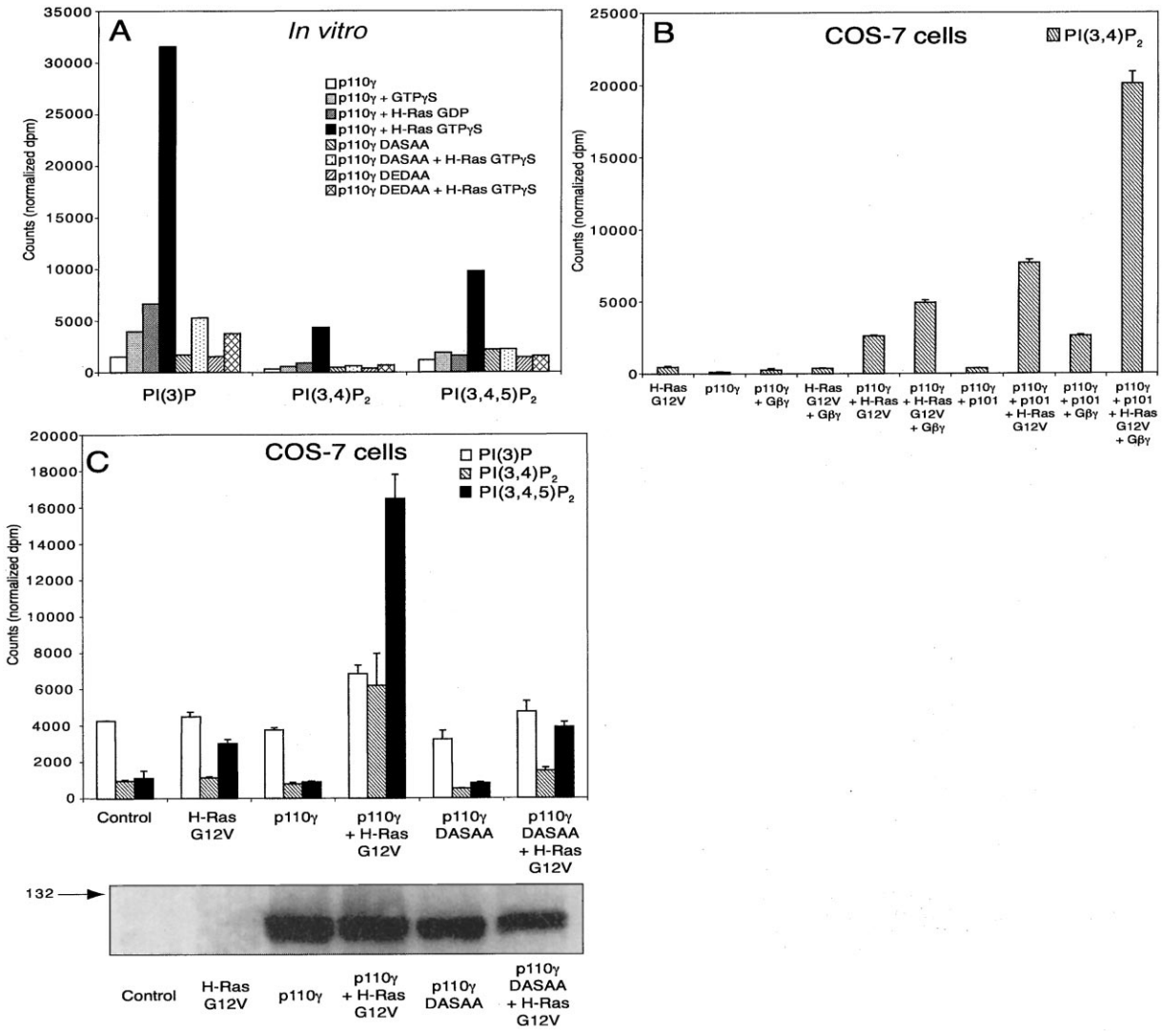

Figure 1. Direct Activation of PI3Kγ by H-Ras

(A) In vitro activation of PI3Kγ by posttranslationally modified, EE-tagged H-Ras·GTPγS using pig neutrophil membranes as a substrate. ^{32}P-labeled phosphoinositides were extracted, deacylated, separated by HPLC, and measured by scintillation counting. The data for [^{32}P]-PtdIns(3)P, [^{32}P]-PtdIns(3,4)P_2, and [^{32}P]-PtdIns(3,4,5)P_3 are shown. Descriptions of the DASAA and DEDAA mutants are in the Experimental Procedures. The data are representative of three experiments and were normalized by the amount of PI3Kγ used in the assay.

(B) In vivo activation of myc-tagged p110γ and the myc-p110γ / EE-tagged p101 heterodimer by H-Ras G12V, and coactivation of myc-p110γ/EE-p101 heterodimer with Gβγ and H-Ras G12V. The error bars represent the range of two experiments.

(C) In vivo activation of untagged wild-type and DASAA mutant p110γ by H-Ras G12V in the absence of p101. COS-7 cells were transfected with expression vectors containing the indicated genes. The levels of ^{32}P-labeled phosphoinositides were normalized to 2×10^5 counts of PtdIns(4)P. The error bars represent the range of two experiments. A Western blot of the cell lysates with an anti-p110γ antibody shows similar expression of p110γ. A Western blot with anti-Ras antibody shows similar expression of Ras (not shown).

against the catalytic domain. Here, we show that Ras forms a transient complex with PI3Kγ and activates it in vitro and in vivo. To characterize the PI3K interaction with Ras, we have trapped a Ras·PI3Kγ complex and determined its structure by X-ray crystallography. This Ras complex with PI3Kγ shows interactions that are unique to PI3K, and is probably also a good model for the interaction of PI3Kα with Ras. The conformational changes that take place in PI3Kγ upon Ras binding are consistent with the possibility that an allosteric mechanism, in addition to membrane recruitment, may be important in the activation of PI3K. Our complex of Ras with PI3Kγ provides a glimpse into the structural ramifications of Ras binding in the context of a full-length effector enzyme.

Results and Discussion

Ras·GTP Directly Activates PI3Kγ

To determine the consequences of Ras binding to PI3Kγ, we investigated the effect of full-length, lipid modified, GDP- or GTPγS-loaded H-Ras on PI3Kγ activity in vitro, using a plasma-membrane enriched membrane preparation from neutrophils. Our results indicate

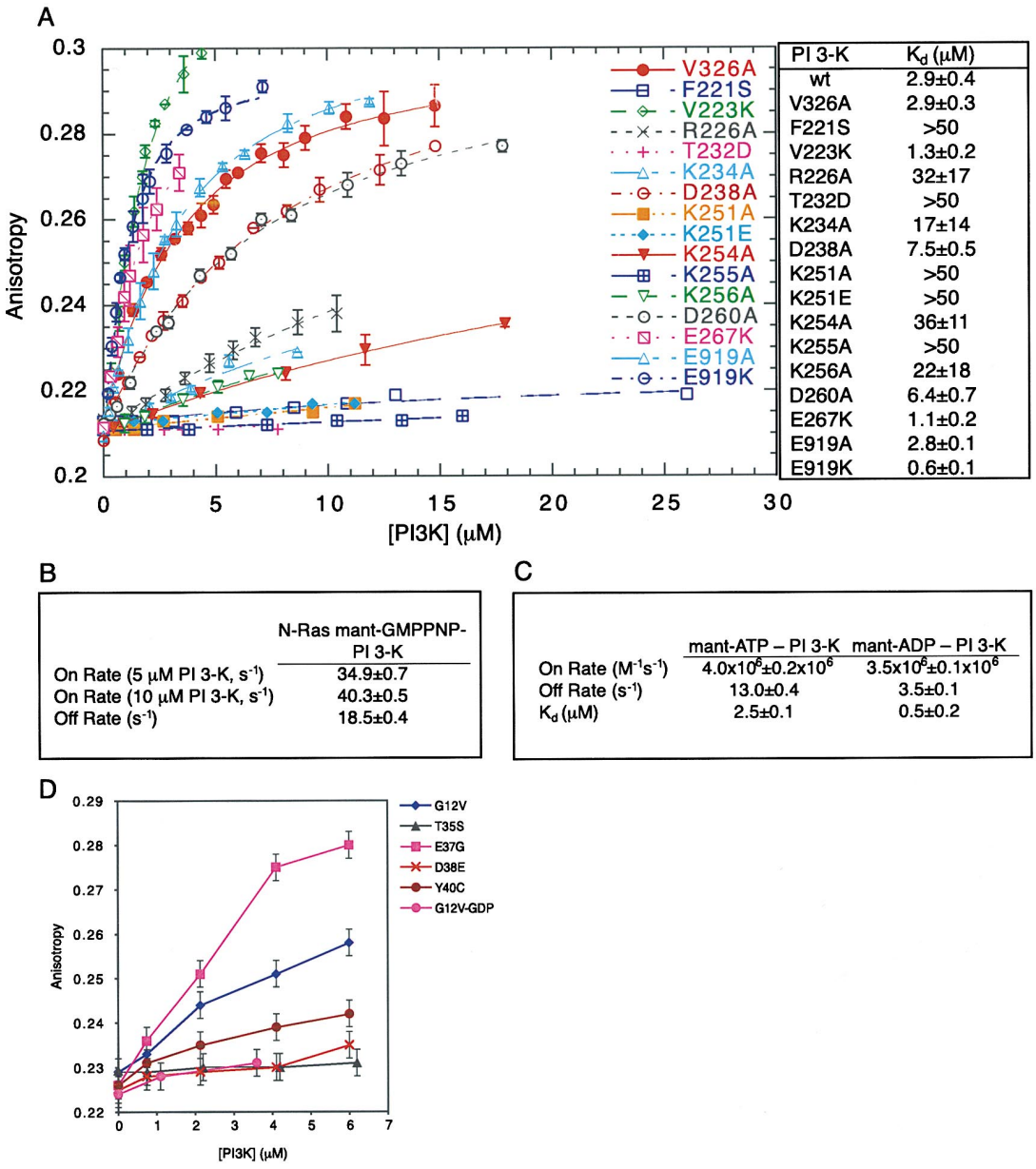

PI 3-K	K_d (μM)
wt	2.9±0.4
V326A	2.9±0.3
F221S	>50
V223K	1.3±0.2
R226A	32±17
T232D	>50
K234A	17±14
D238A	7.5±0.5
K251A	>50
K251E	>50
K254A	36±11
K255A	>50
K256A	22±18
D260A	6.4±0.7
E267K	1.1±0.2
E919A	2.8±0.1
E919K	0.6±0.1

	N-Ras mant-GMPPNP-PI 3-K
On Rate (5 μM PI 3-K, s^{-1})	34.9±0.7
On Rate (10 μM PI 3-K, s^{-1})	40.3±0.5
Off Rate (s^{-1})	18.5±0.4

	mant-ATP – PI 3-K	mant-ADP – PI 3-K
On Rate ($M^{-1}s^{-1}$)	$4.0x10^6$±$0.2x10^6$	$3.5x10^6$±$0.1x10^6$
Off Rate (s^{-1})	13.0±0.4	3.5±0.1
K_d (μM)	2.5±0.1	0.5±0.2

Figure 2. Binding of PI3Kγ to Ras

(A) Solution binding of PI3Kγ RBD mutants (144–1102 constructs) to N-Ras·mant-GMPPNP as measured by fluorescence anisotropy. Titration of some mutants was limited by reduced mutant solubility. All error bars represent the standard deviation of at least two measurements. K_d values are listed in the adjacent table. For mutants with no detectable binding, the K_d is listed as >50.

(B) Transient kinetic measurements of the association and dissociation rates of the PI3Kγ 144–1102 construct to N-Ras·mant-GMPPNP. The pseudo first-order association rates were determined at the PI3Kγ concentrations shown.

(C) Transient and steady-state measurements of mant-ATP and mant-ADP binding to PI3K. All data were collected by fluorescence energy transfer from tryptophan to mant. The K_d values were determined by equilibrium titrations.

(D) Steady-state binding of PI3Kγ (144–1102 construct) to full-length, unprocessed H-Ras mutants. The data were obtained as in Figure 2A. For comparison, PI3Kγ binding to H-Ras G12V·mant-GDP is shown.

that H-Ras·GTPγS causes an approximately 8- to 20-fold increase in the activity of the p110γ catalytic subunit (Figure 1A). This activation is strictly dependent on Ras·GTPγS, and is at least as great as the reported stimulation of the p110α/p85 heterodimer by Ras (Rodriguez-Viciana et al., 1996b). Based on our structure of a complex of PI3Kγ with Ras (see below), we constructed two p110γ variants in which several residues essential for Ras binding were mutated. These multiple mutants (DASAA and DEDAA, see Experimental Procedures) have the same basal activity as the wild-type enzyme in vitro, but are not activated by H-Ras·GTPγS (Figure 1A). These results demonstrate that H-Ras directly activates PI3Kγ.

Previously, it was reported that PI3Kγ is not stimulated by Ras in COS-7 cells (Rubio et al., 1997). Because of

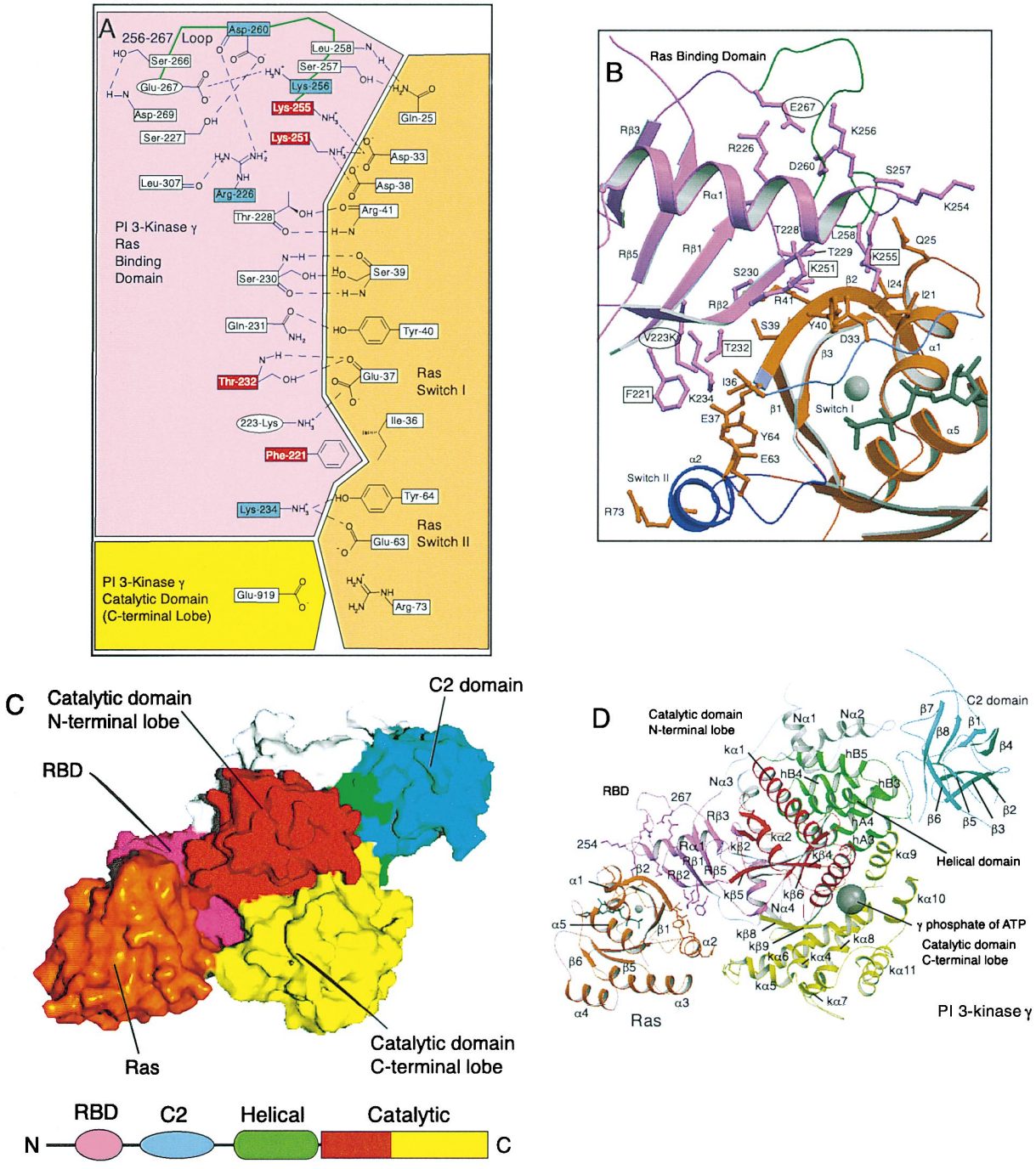

Figure 3. Structure of a Ras·PI3Kγ Complex

(A) Diagram of the PI3Kγ·Ras interface. Also shown are the residues that hold the 255–267 loop in place. The RBD is colored purple, the Ras is orange, and the catalytic domain is yellow. Putative hydrogen bonds are indicated by dashed lines, and possible salt bridges by dotted lines. PI3Kγ residues that can be mutated to eliminate or attenuate binding are colored red or blue, respectively. Ellipses indicate residues that were mutated to enhance binding. The V223K tighter binding mutant is shown hydrogen bonding to Ras Glu37.

(B) A closer view of the interface between the RBD (purple) and Ras (orange). The switch I and switch II regions of Ras are colored pale and dark blue, respectively. Boxes around residue labels denote mutations that abolish binding, and ellipses indicate mutations that enhance binding. The 255–267 loop that becomes ordered on binding is colored dark green. The GMPPNP and Mg^{2+} in Ras are rendered in gray.

(C) Molecular surface of the Ras·PI3Kγ complex. The Ras (orange) and four domains of the PI3Kγ, comprising the RBD (purple), C2 domain (cyan), helical domain (green), and N- and C-terminal lobes of the catalytic domain (red and yellow) are shown. The N-terminal linker is rendered in white. A schematic of PI3Kγ domain organization is also shown.

(D) Ribbon diagram of the Ras·PI3Kγ complex. The color scheme is the same as the previous panel. The location of the γ phosphate of the ATP·PI3Kγ structure is marked with a large gray sphere. This location roughly corresponds to the phosphoinositide headgroup binding site.

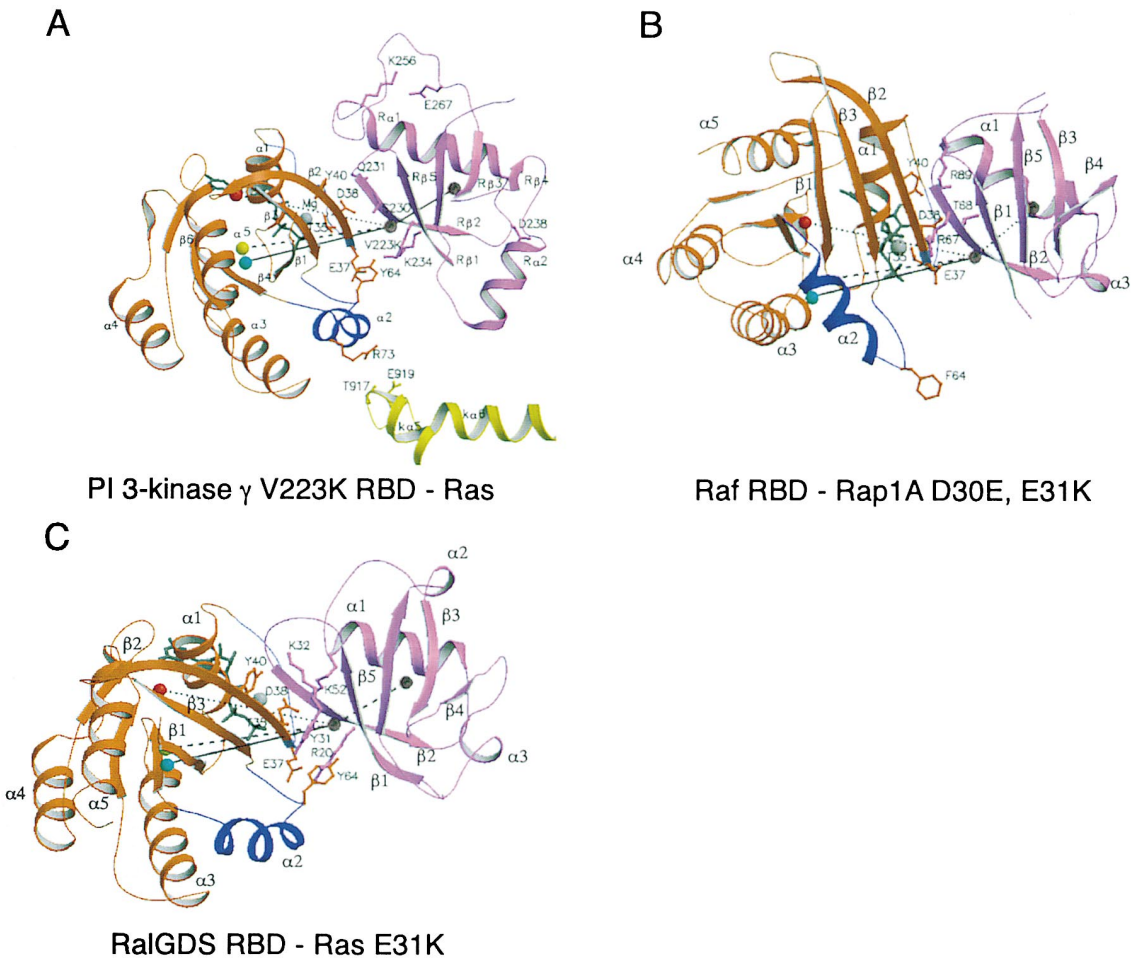

Figure 4. A Comparison of the Ras or Rap1A Orientations in Complexes with the RBDs from PI3K, Raf, and RalGDS

The RBDs were automatically superimposed using the "brute" option of LSQMAN (Kleywegt, 1999). The molecules are colored as in Figure 3. To help visualize the different orientations of bound Ras, lines are traced from the centroid of the RBD through the Cα of Thr232 in PI3Kγ (or its equivalent in other RBDs), then to the centroid of Ras bound to PI3Kγ (cyan sphere and solid line), Raf (red sphere and dotted line), and RalGDS (yellow sphere and dashed line). (A) The PI3Kγ RBD·Ras complex. (B) The Rap1A·RafRBD complex (PDB:1gua). (C) The Ras·RalGDS RBD complex (PDB:1lfd). The orientation of the Ras in this complex is more similar to that of Ras in the PI3Kγ complex than that of Rap1A in the RafRBD complex.

this apparent inconsistency with the in vitro activation that we observed, we reexamined this issue of in vivo activation. We transfected COS-7 cells with various combinations of expression vectors encoding H-Ras G12V, full-length p110γ, p101, $G\beta_1$, and $G\gamma_2$. These data indicate that p110γ alone, and the p101/p110γ heterodimer, are activated 23- and 20-fold, respectively, by H-Ras G12V (Figure 1B). In the presence of Gβγ, H-Ras further stimulates both p110γ and p101/p110γ by 22- and 8-fold above the level produced by Gβγ stimulation (Figure 1B). As in the in vitro experiments, the DASAA Ras binding– deficient p110γ mutant was insensitive to H-Ras G12V, although it was comparably expressed in COS-7 cells (Figure 1C). The effect of H-Ras G12V on p110γ activity in COS-7 cells was completely insensitive to pretreatment with U0126, a potent ERK pathway inhibitor (the inhibitor resulted in a 92% decrease in MAPK activity; data not shown). These results indicate that stimulation of p110γ activity by H-Ras G12V in COS-7 cells is the consequence of a direct interaction between H-Ras and p110γ. The discrepancy between our results and those previously published may be due to differences in the constructs used for the transfections.

PI3Kγ Forms a Transient Complex with Ras·mant-GMPPNP

We characterized the solution binding of PI3Kγ to Ras by observing changes in the fluorescence anisotropy of full-length, unmodified N-Ras·mant-GMPPNP (mant, 2′-(or-3′)-O-(N-methylanthraniloyl)). The K_d for wild-type PI3Kγ and N-Ras·mant-GMPPNP is 2.8 ± 0.4 μM. The K_d for wild-type H-Ras (3.2 ± 0.5 μM) is nearly identical to the K_d for N-Ras. This dissociation constant is higher than the 160 nM K_d for the Ras·Raf RBD complex (Herrmann et al., 1995; Sydor et al., 1998) and the 1 μM K_d for the Ras·RalGDS RBD complex (Herrmann et al., 1996). It is also approximately 10-fold higher than the previously published dissociation constant for PI3Kγ and Ras (Rubio et al., 1999). The discrepancy between our results and those reported previously for p110γ may be due

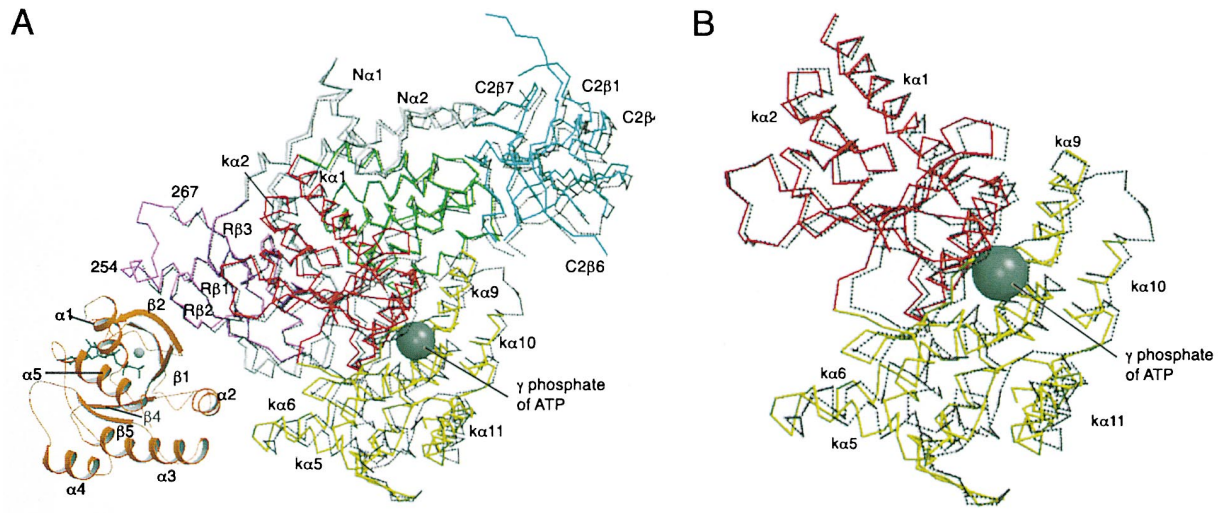

Figure 5. Conformational Changes in the Ras·PI3Kγ Structure

(A) The structure of PI3Kγ bound to ATP is traced through the Cα's as a black dotted line. The structure of the Ras·PI3Kγ complex is traced in a solid line and the domains are colored as in Figure 3. A gray sphere marks the location of the γ-phosphate of ATP in the structure of the enzyme in the absence of Ras. This would presumably be adjacent to the phospholipid headgroup binding site.

(B) A view of the conformational changes in the catalytic domain. The free and Ras-bound PI3Kγ catalytic domains were superimposed using their N-terminal lobes.

to differences in the constructs and methods used to determine the dissociation constants. The previously published work used pull-down assays with an immobilized GST-PI3Kγ construct.

Although the solution K_d for the PI3Kγ·Ras complex is high, it would be sufficient for interaction of the two proteins on lipid membranes. A similar situation is apparent for other signaling complexes that are active at membrane surfaces. For example, the estimated affinity of phospholipase $C\beta_2$ ($PLC\beta_2$) for the Gβγ subunits in the bulk phase is about 3 μM (Runnels and Scarlata, 1998), yet Gβγ is one of the principal activators of $PLC\beta_2$ in cells. Because $PLC\beta_2$ and Gβγ subunits have high affinities for membrane, these signaling components become concentrated on membrane surfaces. Consequently, even fairly weak interactions lead to lateral association on the membrane. PI3Kα and PI3Kγ (Barnett et al., 1995 and S. Krugmann and L. S., unpublished data) have been shown to bind to phosphoinositide-containing membranes even in the absence of any other protein components. Therefore, the bulk affinities that we measure for soluble Ras may translate into a significant interaction with membrane-localized Ras. This is consistent with our observation that the K255A mutant is activated by H-Ras G12V to half of the extent of the wild-type p110γ in COS-7 cells (data not shown) despite having an affinity for soluble N-Ras·mant-GMPPNP that was so weak that it could not be measured by fluorescence anisotropy.

Dynamic studies of PI3Kγ and N-Ras indicate both rapid association and dissociation of the two proteins (Figure 2B). While the dissociation rate of the complex is similar to that of Ras·Raf RBD, the association rate of PI3Kγ·Ras is an order of magnitude slower (Sydor et al., 1998). The dissociation rate constant of the Ras·PI3K complex (>18 s^{-1}) is at least an order of magnitude higher than the maximal catalytic turnover rates for PtdIns(3,4,5)P_3 that have been reported for PI3Kγ (0.1 s^{-1}; Maier et al., 1999) or for PI3Kα (0.8 s^{-1}; Carpenter et al., 1990). As with the Ras·Raf complex, the "activating" interaction of PI3Kγ with Ras is limited by the dissociation of the Ras·effector complex and not by the catalytic cycle of the effector enzyme. The transience of the complex ensures that PI3Kγ is not constitutively activated.

Structure of a Ras·PI3Kγ Complex

Initial crystallization trials of Ras·PI3Kγ were unsuccessful, perhaps because of the transience of the complex. Therefore, we constructed two tighter binding PI3K mutants, V223K and E267K, for cocrystallization with Ras. The K_ds for Ras·GMPPNP of these and other mutants discussed below are shown in Figure 2A. Neither the wild-type protein, the pseudo wild type (V326A, see Experimental Procedures), nor the V223K mutant exhibit detectable binding to N-Ras·GDP, consistent with the role of PI3Kγ as an effector (data not shown). With the V223K mutant, we obtained crystals of the Ras·PI3Kγ complex.

The overall organization of the PI3Kγ catalytic subunit (Walker et al., 1999), which contains a Ras binding domain (RBD), a C2 domain, a helical domain, and a catalytic domain, is preserved in the structure of the complex (Figure 3). PI3Kγ, Raf, and RalGDS interact with many of the same switch I residues of Ras. However, a unique feature of the PI3Kγ·Ras complex is that the switch II region is also involved. Interactions with Ras switch II residues have previously only been observed in complexes of Ras with its upstream regulators, GTPase activating proteins (Scheffzek et al., 1997) and guanine nucleotide exchange factors (Boriack-Sjodin et al., 1998).

One prominent feature of the interaction with Ras is the ordering of a loop, residues 255 to 267, in the RBD (Figure 3B), that is not visible in the free PI3Kγ structure, but is clearly defined in the electron density of the com-

plex. This loop prevents Ras from binding to the PI3Kγ RBD in the same orientation as Ras bound to Raf and RalGDS. Consequently, Ras establishes novel switch II contacts with the PI3Kγ RBD and catalytic domain.

Ras Binding Induces Ordering of a Critical Loop at the RBD·Ras Interface

The entropic cost of locking the PI3Kγ 255–267 loop into a single conformation might be offset by interactions formed between residues in the loop, and between the loop and the rest of the RBD. Eliminating these interactions or providing additional ones would affect the stability of the loop, and concomitantly decrease or increase the affinity of Ras for the kinase. In support of this hypothesis, the PI3Kγ mutants R226A, K256A, and D260A all eliminate hydrogen bonds or salt bridges that stabilize the 255–267 loop (Figure 3A), and reduce binding up to 10-fold (Figure 2). The side chain of another attenuating mutant, Lys254, points away from the Ras. Nevertheless, mutation of this residue to Ala greatly lowers the affinity of PI3Kγ for Ras, possibly by permitting more flexibility in the turn containing the critical residues Lys255 and Lys256. The complex-stabilizing E267K mutant would permit the formation of an additional hydrogen bond from the mutant Lys267 to the backbone amide oxygen of Phe249, which could further stabilize the 255–267 loop and helix Rα1. Apparently, this also offsets any destabilization that arises from placing Lys267 and Lys255 fairly near each other on the surface of the protein.

The Switch I Region of Ras Forms Typical Effector Interactions with PI3K

At the interface between Ras and the PI3Kγ RBD, strand β2 of Ras is aligned with PI3Kγ strand Rβ2 (Figure 3B). This produces a continuous antiparallel β sheet between the Ras and the RBD. The interaction is common to structures of Rap1A and Ras in complexes with Raf-RBD and RalGDS-RBD, respectively (Nassar et al., 1995; Huang et al., 1998; Vetter et al., 1999). Most of the interactions between Ras and PI3Kγ are either hydrogen bonds or salt bridges (Figure 3A), in agreement with the observation that the affinity of the two proteins is inversely related to the ionic strength of the buffer (data not shown). The area of the interface between the PI3Kγ RBD and Ras (1308 Å^2) is similar to the surface areas of the Raf RBD (1333 Å^2) and RalGDS RBD (1331 Å^2) interfaces.

The effects of several PI3Kγ mutations that we made in the RBD·Ras interface are consistent with their apparent roles in forming switch I contacts. The T232D, K251A/E, and K255A mutations all eliminate binding by removing hydrogen bond donors or acceptors from the Ras switch I·PI3Kγ interface, and in the case of the T232D and K251E mutations, by putting negatively charged PI3Kγ side chains into proximity with negatively charged side chains in Ras (Figure 3A). K251E is the equivalent of the K227E mutant in PI3Kα, which also eliminates Ras binding (Rodriguez-Viciana et al., 1996b; Bondeva et al., 1998). The mechanism of the tighter binding V223K mutant can be explained in terms of interaction with the switch I region, because this mutation permits formation of an additional hydrogen bond between the RBD Lys223 and Ras Glu37.

Ras Makes Essential Interactions with PI3K Using Its Switch II Region

Unlike any other effectors downstream of Ras, PI3Kγ makes critical interactions with the switch II region. Although early structural studies of Ras showed that both switch I and switch II regions of Ras changed conformation upon GTP binding, and transforming mutants of Ras involving both of these regions have been reported, the structures of other effector RBDs in complexes with Ras showed only switch I interactions. In the PI3Kγ·Ras complex, we observe extensive switch II contacts that are probably the consequence of the unique orientation of Ras relative to the RBD of PI3Kγ. We have generated two mutants, F221S and K234A, involving residues that make switch II contacts. F221S eliminates hydrophobic interactions between PI3Kγ Phe221 and Tyr64 in switch II. Mutation of Lys234 to Ala probably increases the K_d by eliminating hydrogen bonds to switch II residues Glu63 and Tyr64 (Figure 3A). These mutants confirm the essential role of Ras Switch II in binding PI3Kγ. In addition, the Y64G Ras mutation abolishes binding of a class IA PI3K (Moodie et al., 1995), suggesting that interaction with the Ras switch II is probably a general characteristic of PI3K·Ras complexes.

The PI3K Catalytic Domain Makes Direct Interactions with Switch II of Ras

Ras directly contacts the C-terminal lobe of the PI3Kγ catalytic domain. Arg73 in the switch II region of Ras is near Glu919 in the turn between helices kα5 and kα6. The E919A mutant shows wild-type affinity for Ras; however, the E919K mutation greatly increases affinity for Ras (Figure 2A), presumably by forming a new salt-link between the catalytic domain and Asp69 in switch II of Ras. This suggests that the close approach of Ras to the catalytic domain that we see in the structure is not simply an artifact of crystal packing. This direct contact between the PI3K catalytic domain and Ras may contribute to the conformational change in the phospholipid binding site of PI3Kγ (see below).

Ras Binds to RBDs in Effector-Specific Orientations

Two structures of isolated RBD complexes with Ras or the Ras-like protein Rap1A have been previously solved. In Figure 4, the Raf RBD·Rap1A complex (Nassar et al., 1995) and the RalGDS RBD·Ras complex (Huang et al., 1998) are compared with the PI3Kγ·Ras complex.

All three Ras·RBD complexes use a similar general mode of Ras-effector interaction, in which a β sheet in the Ras and a β sheet in the RBD are aligned to form a single β sheet connecting the two proteins. Contacts between the switch I region of Ras and the RBD stabilize the interaction and ensure its dependence on Ras-GTP.

Despite the common mode of the Ras·RBD interaction, Ras discriminates among its effectors by rotating with respect to the RBD of a given effector. Ras bound to PI3Kγ is rotated by 35° relative to the centroid of Rap1A bound to the Raf RBD, and by 17° relative to Ras bound to the RalGDS RBD (Figure 4A). In PI3Kγ, the

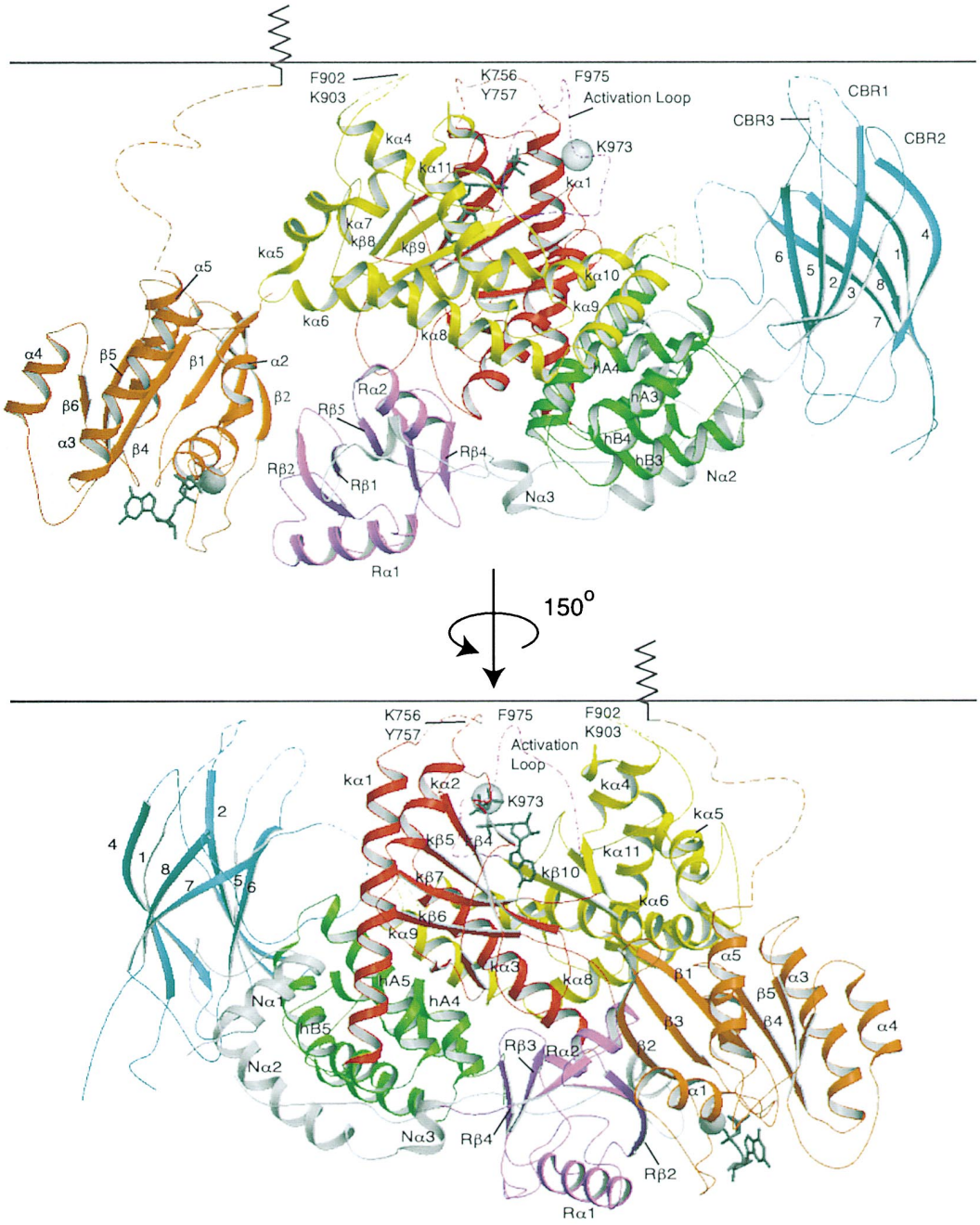

Figure 6. A Putative Model of the Ras·PI3Kγ Complex at a Membrane Surface

All regions not visible in the structure are drawn as dashed lines. Lys973 marks the substrate binding loop. The 20 residue C-terminal tail of Ras was arbitrarily modeled to illustrate that this peptide could easily span the gap between the RBD-bound Ras and the putative membrane surface. The location of the farnesyl group is indicated schematically. Potential membrane-interacting residues at the tips of the catalytic domain loops are labeled.

length of helix Rα1 and the size of the subsequent loop (255–267) cause a significant rotation of Ras relative to the PI3Kγ RBD and results in switch II interactions, for which there are no equivalents in the other Ras effector RBDs. The 255–267 loop appears longer in PI3Kγ and α than in PI3Ks β and δ. This is in agreement with the observation that PI3Kδ appears to differ from PI3Kα in its interaction with Ras (Kinashi et al., 2000).

Structural Insights into Signaling Pathway–Specific Ras Mutations

Five Ras mutants have been defined that differentially affect Raf, RalGDS, and PI3Kα signaling pathways. These mutants, T35S, E37G, D38E, Y40C, and Y64G, have served as useful tools for unraveling networks of signal transduction pathways (White et al., 1995; Rodriguez-Viciana et al., 1997). The selective activation dis-

played by the switch I mutants (T35S, E37G, D38E, and Y40C) appears to be due to subtle differences in the network of interactions that the switch I region makes in the three Ras/effector complexes. For the switch II mutant (Y64G), PI3K activation is probably selectively abrogated simply because PI3K forms a switch II contact whereas the other effectors do not (Vetter et al., 1999).

E37G is a Ras mutant that activates RalGDS but not Raf. Although this mutant does not bind to or activate PI3Kα, it was recently shown to activate PI3Kδ (Kinashi et al., 2000). We find that, as with PI3Kδ, PI3Kγ binds Ras E37G similarly to wild-type Ras (Figure 2D). Glu37 of Ras forms only a weak ionic interaction with RalGDS, while it forms two hydrogen bonds with the guanidinium group of Arg59 in Raf. Although we see a salt link between PI3Kγ Lys223 and Ras Glu37 in the structure of the V223K mutant, this interaction would not be possible with the wild-type PI3Kγ, consistent with the unimpaired binding of PI3Kγ to the Ras E37G mutant. The residue in PI3Kα at the position equivalent to PI3Kγ Val223 is also a Val (Val193). This suggests that in PI3Kα another residue in the vicinity of Val193 interacts with Ras Glu37. One candidate for such a residue is Lys206 of PI3Kα. Neither PI3Kγ nor PI3Kδ have a basic residue at the equivalent position.

D38E and T35S are Ras mutants that selectively activate the Raf signaling pathway. PI3Kα (Rodriguez-Viciana et al., 1997), PI3Kδ (Kinashi et al., 2000), and PI3Kγ (Figure 2D) all show considerably reduced binding to these mutants. It is not clear from the structure why the T35S mutant eliminates PI3K binding. Asp38 makes important contacts with the RBDs of all three effectors and D38A prevents Ras activation of these pathways. The D38E mutation conserves the negative charge, but it introduces a larger residue into the intricate interface. This is only tolerated in Raf because Thr68 of Raf leaves sufficient space in the vicinity of the side chain of Ras residue 38. In PI3Kγ, the bulky Gln231 occupies the space analogous to Thr68 of Raf and prevents Ras D38E binding, while in RalGDS, this space is filled by Lys32. In PI3Kα and PI3Kδ, a bulky residue (Tyr207 and Phe203, respectively) also occupies this space.

One Ras mutation that has been used widely to selectively activate PI3Kα is the Y40C mutation. Surprisingly, this mutation eliminates binding to PI3Kδ (Kinashi et al., 2000) and attenuates binding to PI3Kγ (Figure 2D). Tyr40 forms a putative hydrogen bond to Gln231. Mutation of Tyr40 to Cys probably eliminates this potential hydrogen bond and reduces PI3Kγ binding. Since Gln231 is not conserved in PI3Kα, the hydrogen bond between Ras Tyr40 may not be present, and the Y40C mutation would not affect binding. In complexes with Raf and RalGDS, the role of Ras Tyr40 appears to be to restrict the motion of a nearby basic residue in the RBD (Arg89 in Raf and Lys32 in RalGDS), which forms a critical salt bridge with Ras Asp38.

The Ras mutant Y64G selectively inhibits PI3K and neurofibromin binding (Moodie et al., 1995). Ras Tyr64 in switch II forms an apparent hydrogen bond to the side chain of Lys234 and makes hydrophobic contacts with Phe221 of PI3Kγ. These interactions would be lost in the Y64G mutant. Tyr64 also stacks with the carboxylate of Ras Glu63, which forms a hydrogen bond with Lys234. In contrast, neither Raf nor RalGDS RBDs contact any residues in switch II (Nassar et al., 1995; Vetter et al., 1999).

Conformational Change in the Ras·PI3Kγ Complex

In addition to the induced fit of residues 255–267 at the interface with Ras, the structure of the Ras·PI3Kγ complex demonstrates that there are other more widespread conformational changes relative to the structure of the enzyme in the absence of Ras. Most of the conformational change, as illustrated in Figure 5A, occurs in the C2 domain and the C-terminal lobe of the catalytic domain. When the structure of the free PI3Kγ and the structure of the complex are superimposed on the Ras binding domain, the RMS deviation of the Cα atoms for the C2 domain is 1.7 Å. The RMS deviation of the Cα atoms for the C-terminal lobe of the catalytic domain is 1.9 Å. The maximum deviation is 4.6 Å at the Cα of Pro916, which is located between helices kα5 and kα6 in the C-terminal lobe of the catalytic domain. These values are well outside the cross-validated σ_A estimate of the error of the atom positions, which is 0.7 Å (based on the free set of reflections). Neither the N-terminal lobe of the catalytic domain nor the overall RBD show significant conformational change. The deviation of the helical domain in the structure of the complex from the free PI3Kγ structure is probably due to proteolysis in this domain (see Experimental Procedures).

In PI3Kγ, the ATP binding site is located between the N- and C- terminal lobes of the catalytic domain. As in the protein kinases (Zhou and Adams, 1997), mant-ADP release is slower than mant-ATP release (Figure 2C). In the Ras·PI3Kγ complex, helix kα6 in the C-terminal lobe of the catalytic domain is pulled toward the Ras, and the entire ATP binding site moves with it, but apart from Asp964, none of the residues in the ATP binding site significantly change conformation. Consistent with this observation, neither the dissociation rate constants nor the K_d for either mant-ATP or mant-ADP change in the presence of Ras (data not shown).

Unlike the ATP binding pocket, the putative phosphoinositide headgroup binding site appears to substantially change conformation upon Ras binding, as the C-terminal lobe of the catalytic domain pivots around the N-terminal lobe (Figure 5B). Unfortunately, we have been unable to grow crystals in the presence of a phospholipid headgroup analog, so we cannot be sure of the detailed structural changes relevant to headgroup binding. The backbones of helices kα9, kα10, and kα11, as well as kβ10 and kα7, which hold the activation loop in place, all substantially change position. Any allosteric mechanism of activation would probably involve a change in the affinity of phospholipid substrate binding, or perhaps an increase in the k_{cat} of the enzyme.

Although we cannot rule out proteolysis of the enzyme or crystal packing as the cause of the conformational changes that we see, the consistency of the biochemical and structural data suggests that this structure demonstrates a potential mode of Ras-induced conformational changes in PI3Kγ.

A Model for Ras Activation of PI3K

The structure of the Ras bound to PI3Kγ was used to construct a model of the activated complex on a lipid

Table 1. Data Collection, Structure Determination, and Refinement Statistics

[1]Data set	Resolution (Å)	Observations/ unique reflections	Completeness (last shell) (%)	R_{sym}[2]	$\langle I/\sigma \rangle$ (last shell)
Crystal 1	50–3.2	146,371/23,318	100 (100)	0.11	21.8 (3.6)
Crystal 2[3]	50–3.0	270,093/24,791	82.4 (51.3)	0.094	14.7 (1.7)
Merge[4]	50–3.0	232,825/25,822	91.6 (50.5)	0.10	20.0 (1.7)

Refinement statistics

Data set	Resolution (Å)	Protein atoms	Waters	Reflections Work	Reflections Free	R_{cryst}[5]	R_{free}[5] (% data used)	Rmsd from ideality[6] Bonds	Angles	Dihedrals
Merge	50–3.0	7405	6	24,273	1510	0.21	0.28 (5.4)	0.0093 Å	1.29°	22.7°

[1] The data from crystals 1 and 2 were collected at ESRF Beamline ID14-1.
[2] $R_{sym} = \Sigma_{hkl}\Sigma_i|I_i(hkl) - \langle I(hkl)\rangle|/\Sigma_{hkl}\Sigma_i I_i(hkl)$.
[3] Only 50 degrees were collected due to radiation damage caused by long exposure.
[4] The merged dataset was created by combining the data from crystals 1 and 2 in SCALA.
[5] R_{cryst} and $R_{free} = \Sigma|F_{obs} - F_{calc}|/\Sigma F_{obs}$; R_{free} calculated with the percentage of the data shown in parentheses.
[6] Rms deviations for bond angles and lengths in regard to Engh & Huber parameters (Engh and Huber, 1991).

membrane. When the PI3Kγ active site is oriented toward the membrane surface and the C2 domain is binding phospholipids, the 20 residue tail of Ras (not present in the Ras construct used for crystallization) has ample length to span the gap between the Ras effector domain and its farnesyl membrane anchor (Figure 6). The loops of the PI3Kγ catalytic domain near the putative membrane interface contain basic residues which could bind negatively charged phospholipid headgroups and hydrophobic residues capable of inserting into the membrane to help tether the enzyme in place.

In the Ras·PI3Kγ complex, the C2 and catalytic domains are slightly spread apart from each other (Figure 5A), presenting the active site to the membrane. This structural change may affect phosphoinositide binding in the active site, or increase the general affinity of the enzyme for the membrane interface. Although a substantial component of the Ras activation of PI3Kγ could be via translocation to the membrane, an allosteric mechanism, as suggested by the conformational change, may also be a component of Ras activation.

The costimulation of PI3Kγ by G$\beta\gamma$ and Ras is consistent with the emerging view of PI3Ks as integrators of multiple signaling pathways. The success of our design of both complex-stabilizing and destabilizing mutants, in conjunction with the novel interactions observed in the Ras·PI3Kγ structure, suggest new possibilities for the design of PI3K and Ras variants to control specific signal transduction pathways.

Experimental Procedures

Protein Cloning and Expression

For crystallography, equilibrium binding, and kinetic measurements, a construct containing residues 144–1102 of the human PI3Kγ with a C-terminal His_6 tag was cloned into pVL1393 (Invitrogen) for baculovirus expression. To make the RBD mutants, we used a cassette containing a V326A mutation, which encoded a NheI site used for subcloning. This V326A "pseudo wild-type" construct has the same affinity for N-Ras as the wild-type protein (Figure 2A). The DASAA PI3Kγ mutant used for the in vitro and in vivo experiments contains the T232D, K251A, K254S, K255A, and K256A mutations in the context of the full-length pseudo wild-type p110γ subunit. The DEDAA mutant contains the T232D, K251E, K254D, K255A, and K256A mutations. For expression in COS-7 cells, the DASAA and DEDAA mutants were subcloned into pcDNA3 with no tags. For in vitro Ras activation studies, the DASAA and DEDAA mutants were subcloned into pVL1393 with a C-terminal His_6 tag.

PI3K constructs in pVL1393 were transfected into Sf9 cells with BaculoGold DNA (Pharmingen). Infected cells were incubated at 27°C for 48 hr. Harvested cells were washed in PBS, pelleted, frozen in liquid nitrogen, and stored at −80°C.

The DNA sequence encoding residues 1–166 of *H. sapiens* H-Ras G12V was cloned as a NdeI/BamHI fragment into pET11a (Novagen) and transformed into C41(DE3) cells. For expression, bacteria were grown at 37°C to an OD_{600} of 0.7, and induced with 100 μM IPTG for 12 hr. Full-length, his-tagged H-Ras mutants (a gift from J. Downward) were grown in a similar manner and induced for 5 hr with 500 μM IPTG.

Protein Purification

P110γ proteins were purified using immobilized metal affinity, cation exchange, and gel filtration chromatography as previously described (Walker et al., 2000). The proteins were gel filtered in a buffer consisting of 20 mM Tris (pH 7.2), 10–50 mM $(NH_4)_2SO_4$, 1% betaine, 1% ethylene glycol, 0.02% CHAPS, and 5 mM DTT, concentrated to 4–6 mg/mL and snap frozen.

H-Ras 1–166 was extracted from 1 liter of bacterial culture with B-PER reagent (Pierce) and purified by two passages over a HiLoad Q column (Pharmacia) with a salt gradient (0–1 M KCl in 50 mM Tris [pH 7.5], 1 mM $MgCl_2$, 5 μM GDP, and 1 mM DTT). The protein was gel filtered on a Superdex 75 column (Pharmacia) in storage buffer (50 mM Tris [pH 7.5], 1 mM $MgCl_2$, 5 μM GDP, and 1 mM DTT), concentrated to 20 mg/mL, and snap frozen. Full-length H-Ras mutants were purified as previously described (Rodriguez-Viciana et al., 1997). H-Ras was loaded with GMPPNP using the alkaline phosphatase protocol as described previously (Herrmann et al., 1996).

Posttranslationally modified H-Ras was obtained by infecting Sf9 cells with a baculovirus encoding EE-tagged H-Ras. Cells were harvested after 2.5 days and sonicated in a buffer consisting of 5 mM $MgCl_2$, 100 mM GDP, 1mM DTT, 5 mM EGTA, 0.15 M NaCl, 40 mM HEPES (pH 7.4) (5°C), and protease inhibitors. Modified H-Ras was separated from unmodified H-Ras by Triton X-114 partitioning and purified by immunoprecipitation with protein G Sepharose coupled to an anti-EE antibody. Proteins were eluted in a buffer containing 1% sodium cholate, 10 μM GDP, 1 mM DTT, 1mM EGTA, 5 mM $MgCl_2$, and eluting peptide (150 μg/ml) as described in Stephens et al., 1997, concentrated to approximately 2–3 mg/ml, and stored at −80°C.

In Vitro and In Vivo Activity Measurements

H-Ras was loaded with GTPγS or GDP by incubation with a 10-fold molar excess of the relevant nucleotide in 5 mM EDTA/5 mM $MgCl_2$. After 20 min at 20°C, $MgCl_2$ was added to a final concentration of 10 mM and the protein was frozen at −80°C.

Pig neutrophil membranes were obtained as described previously (Bennett et al., 1982). Assays were carried out by incubating neutrophil membranes (5 μg protein) with GTPγS or GDP-loaded post-

translationally modified H-Ras (final concentration in assay, 1 μM, with a final cholate concentration of 0.1%) in a buffer containing 0.1 M KCl, 1mM EGTA, 5mM $MgCl_2$, 20mM HEPES (pH 7.5) at 5°C, 1mM DTT (in a total volume of 6 μl) on ice. After incubation for 10 min, 1 μl of PI3K (300 ng) was added; p110γ was stored at 2–4 mg/ml in 20 mM Tris (pH 7.2), 30mM $(NH_4)_2SO_4$, 1% betaine, 1% ethylene glycol, 0.02% CHAPS, and 5 mM DTT and diluted ~10-fold into PBS containing 1mM EDTA and 1mM DTT before addition into the assays. After an additional 5 min, buffer containing [γ-^{32}P]ATP (20 μCi per assay with a final ATP concentration of 200 μM with 1.26 mM $MgCl_2$, 0.1M KCl, 20 mM HEPES (pH 7.5, 5°C), 1mM DTT, and 1mM EDTA) was added and the reactions were transferred to 30°C. After 3 min, the assays were quenched, and the lipids extracted, deacylated, analyzed by HPLC, and quantitated as described previously (Stephens et al., 1997).

COS-7 cells were transfected with plasmid DNA (5–10 μg of full-length PI3Kγ, myc-tagged p101, H-Ras G12V, or an unrelated control DNA for a total of 15–25 μg per transfection in a final volume of 0.5 mL) as described previously (Stephens et al., 1997). After electroporation, the cells were plated in 6 cm diameter dishes and incubated for 36 hr in complete growth medium (DMEM with 10% v/v FBS), washed, and then incubated in HEPES-buffered DMEM containing 1 mM $NaHCO_3$ and 0.2% (w/v) fatty acid-free BSA (starvation medium). After 8 hr, the cells were washed with a phosphate-free version of the starvation medium and incubated for 90 min with 0.25–0.5 mCi [^{32}P]-P_i per dish. For cells treated with U0126, the drug was added to the starvation medium to a final concentration of 10 μM, and was continuously present in the wash and labeling solutions until cell harvesting. The cells were harvested and ^{32}P-labeled phospholipids measured as described previously (Stephens et al., 1997).

Anisotropy Titrations

Mant-nucleotides were synthesized as described previously (Jameson and Eccleston, 1997). N-Ras and H-Ras mutants were loaded with mant-GMPPNP as in Moore et al., 1993, gel filtered into running buffer (20 mM Tris [pH 7.5], 2 mM $MgCl_2$, and 1 mM DTT), and frozen at −80° C. The concentration of Ras·mant-GMPPNP was determined by measuring the absorbance of the mant group at 350 nm with ϵ = 5700 $M^{-1}\,cm^{-1}$ (Hiratsuka, 1983). For binding assays, the 144–1102 human PI3Kγ was titrated into a 1 μM solution of full-length, unmodified N-Ras·mant-GMPPNP. Data were collected with SLM 8000 S and ISS PC1 spectrofluorimeters, set up in the T-format and L-format, respectively, with prism polarizers. All measurements were taken at 20°C with a λ_{ex} of 366 nm. The emission PMTs were fitted with 399 nm cutoff filters. Five measurements of each data point were obtained and averaged. Data were fitted to the binding equation.

Stopped Flow Anisotropy

A Hi-Tech MX61 instrument (Hi-Tech, Salisbury) set up in the T-format with prism polarizers was used to collect data at 20°C. The mant group was excited at 366 nm and emission monitored through 399 nm cutoff filters. The association kinetics were followed by rapid mixing of PI3Kγ with 1 μM N-Ras·mant-GMPPNP under pseudo first-order conditions (PI3Kγ in large excess). Specifically, equal volumes of N-Ras and PI3Kγ were mixed to a final Ras concentration of 1 μM and final PI3Kγ concentrations of 5 and 10 μM. The dissociation rate was measured by mixing a solution of 1 μM N-Ras·mant-GMPPNP and 5 μM PI3K with 9 μM N-Ras·GMPPNP. Attempts to determine association rates at higher PI3K concentrations were limited by solubility of the protein. Data were fitted to single exponential curves within the Hi-Tech software.

Steady State and Kinetic Measurements of ATP and ADP Binding

Equilibrium binding of mant-ATP to PI3K was measured in a SLM 8000 S spectrofluorimeter with λ_{ex} = 280 nm and λ_{em} = 440 nm. This allowed monitoring of energy transfer from tryptophan in the PI3K to mant-ATP. Mant-ATP was titrated into a 1 μM solution of PI3K in running buffer. Each data point represents the average of data collected for 30 s with a 1 s integration time. For data collected in the presence of Ras, the solution also contained 6 μM H-ras·GMPPNP. The data were fitted to the binding equation with Kaleidagraph.

All kinetic data were collected in a Hi-Tech MX61 instrument set up in the single push mode with λ_{ex} = 280 nm and emission monitored with 399 nm cutoff filters. A solution of PI3K was mixed with a solution of mant-ATP such that the final PI3K concentration was 1 μM and the ATP concentrations were 2.5, 5, 7.5, 10, 12.5, and 25 μM. The displacement experiment was carried out by mixing 1 μM PI3K and 2 μM mant-ATP with 50 or 200 μM ATP. Curve fits were carried out with the Hi-Tech software and Kaleidagraph. Equilibrium and kinetic data for mant-ADP were collected by the same methods.

Crystallography

H-Ras·GMPPNP and PI3Kγ (V223K in the context of the 144–1102 pseudo wild-type construct) were mixed to final concentrations of 170 μM for H-Ras and 29 μM for PI3K. The mixture was incubated for 3 days at 17°C, and then set in hanging drops against a reservoir of 50 mM KH_2PO_4/K_2HPO_4 (pH 6.3) and 4.3% PEG 8000. Crystals were propagated by hair seeding and grew to dimensions of 120 μm × 70 μm × 50 μm in 10 days. SDS–PAGE analysis of the crystals showed that the PI3Kγ had been completely digested into four fragments (43, 32, 20, and 10 kDa) during the time course of crystallization. The largest crystals were transferred to cryoprotectant (reservoir with 40% trehalose) in two brief steps and frozen in a liquid N_2 cryostream.

Data sets were collected at beamlines ID14–2 and ID14–1 at the European Synchotron Radiation Facility in Grenoble at a wavelength of 0.934 Å (Table 1). The space group was $P3_121$ with cell dimensions of a = 113.6 Å, c = 183.9 Å, and one complex in the asymmetric unit. The reflections from two crystals were indexed and integrated with MOSFLM (Leslie, 1992), merged, and scaled with SCALA (CCP4, 1994). Molecular replacement was carried out with AMoRe. The initial model consisted of our human PI3Kγ structure (Walker et al., 2000). A second rotation/translation search with the structure of Ras (Pai et al., 1990) (PDB:5p21) located the Ras molecule. The partial model was rebuilt in O (Jones et al., 1991) and refined with CNS (Brunger et al., 1998). The average B factor is 70 $Å^2$. No residues are in the disallowed regions of the Ramachandran plot. Figures were prepared with MOLSCRIPT (Kraulis, 1991), GRASP (Nicholls et al., 1991), and Raster3D (Merritt and Bacon, 1997).

In the structure, all residues in the Ras are visible. The ordering of the 255–267 loop and better side chain definition at places in the region from 228 to 255 showed that there was a register shift in the fit of the sequence to the electron density in this region in the original structure of PI3K.

As in the previous structure of the free PI3Kγ, several loops are not visible in the electron density. These include the RBD-C2 domain linker (residues 323–352), CBR3 in the C2 domain (residues 436–456), the loop between C2β7 and C2β8 (residues 489–497), the activation loop in the catalytic domain (residues 969–980), and residues1085 to 1102 in the C terminus. Several loops that were defined in the free PI3K are not visible in the electron density of the complex. These include CBR1 (residues 375–378) and loops between residues 754–760, residues 896–901, and residues 1038–1046. It is possible that some of the disordered loops not visible in the electron density also correspond to sites of proteolytic nicking (see above).

The N-terminal half of the helical domain (residues 527–620, containing helices hA1 to hB2′) is not present in the structure. Since the Ras of a symmetry-related complex packs in this space, and SDS-PAGE analysis of the crystals showed no full-length PI3Kγ, this half of the domain was lost to proteolysis during crystallization.

Acknowledgments

We thank Jon Hutchinson for advice on fluorescence anisotropy data collection and analysis, Julian Downward for H-Ras mutants, and Murray Stewart, Andrew Carter, and Michel Goedert for comments on the manuscript. We also thank the staff of beamlines ID14-2 and ID14-1, Ed Mitchell and Julien Lescar, for help in synchrotron data collection. M. P. is supported by a British Marshall Scholarship. S. S. was supported by a BBSRC GAIN Initiative project grant. P. H. was supported by a BBSRC senior fellowship. We are grateful for funding from the British Heart Foundation (R. L. W.).

Received August 18, 2000; revised October 30, 2000.

References

Barnett, S.F., Ledder, L.M., Stirdivant, S.M., Ahern, J., Conroy, R.R., and Heimbrook, D.C. (1995). Interfacial catalysis by phosphoinositide 3′-hydroxykinase. Biochemistry *34*, 14254–14262.

Bennett, J.P., Cockroft, S., Caswell, A.H., and Gomperts, B.D. (1982). Plasma-membrane location of phosphatidylinositol hydrolysis in rabbit neutrophils stimulated with formylmethionyl-leucylphenylalanine. Biochem. J. *208*, 801–808.

Bondeva, T., Pirola, L., Bulgarelli-Leva, G., Rubio, I., Wetzker, R., and Wymann, M.P. (1998). Bifurcation of lipid and protein kinase signals of PI3Kγ to the protein kinases PKB and MAPK. Science *282*, 293–296.

Boriack-Sjodin, P.A., Margarit, S.M., Bar-Sagi, D., and Kuriyan, J. (1998). The structural basis of the activation of Ras by Sos. Nature *394*, 337–343.

Brunger, A.T., Adams, P.D., Clore, G.M., DeLano, W.L., Gros, P., Grosse-Kunstleve, R.W., Jiang, J.S., Kuszewski, J., Nilges, M., Pannu, N.S., et al. (1998). Crystallography & NMR system: A new software suite for macromolecular structure determination. Acta Crystallogr. D *54*, 905–921.

Carpenter, C.L., Duckworth, B.C., Auger, K.R., Cohen, B., Schaffhausen, B.S., and Cantley, L. (1990). Purification and characterization of phosphoinositide 3-kinase from rat liver. J. Biol. Chem. *265*, 19704–19707.

Carpenter, C., Auger, K., Chanudhuri, M., Yoakim, M., Schaffhausen, B., Shoelson, S., and Cantley, L. (1993). Phosphoinositide 3-kinase is activated by phosphopeptides that bind to the SH2 domains of the 85-kDa subunit. J. Biol. Chem. *268*, 9478–9483.

CCP4 (1994). Collaborative Computing Project 4: a suite of programs for protein crystallography, Acta Crystallogr. D *50*, 760–763.

Condliffe, A.M., Hawkins, P.T., Stephens, L.R., Haslett, C., and Chilvers, E.R. (1998). Priming of human neutrophil superoxide generation by tumour necrosis factor-alpha is signalled by enhanced phosphatidylinositol 3,4,5- trisphosphate but not inositol 1,4,5-trisphosphate accumulation. FEBS Lett. *439*, 147–151.

Deora, A.A., Win, T., Vanhaesebroeck, B., and Lander, H.M. (1998). A redox-triggered ras-effector interaction. Recruitment of phosphatidylinositol 3′-kinase to Ras by redox stress. J. Biol. Chem. *273*, 29923–29928.

Domin, J., and Waterfield, M.D. (1997). Using structure to define the function of phosphoinositide 3-kinase family members. FEBS Lett. *410*, 91–95.

Engh, R.A., and Huber, R. (1991). Accurate bond and angle parameters for x-ray protein structure refinement. Acta Crystallogr. A *47*, 392–400.

Feig, L.A., Urano, T., and Cantor, S. (1996). Evidence for a Ras/Ral signaling cascade. Trends Biochem. Sci. *21*, 438–441.

Franke, T.F., Kaplan, D.R., and Cantley, L.C. (1997). PI3K: downstream AKTion blocks apoptosis. Cell *88*, 435–437.

Gire, V., Marshall, C., and Wynford-Thomas, D. (2000). PI-3-kinase is an essential anti-apoptotic effector in the proliferative response of primary human epithelial cells to mutant RAS. Oncogene *19*, 2269–2276.

Herrmann, C., Martin, G.A., and Wittinghofer, A. (1995). Quantitative analysis of the complex between p21ras and the Ras-binding domain of the human Raf-1 protein kinase. J. Biol. Chem. *270*, 2901–2905.

Herrmann, C., Horn, G., Spaargaren, M., and Wittinghofer, A. (1996). Differential interaction of the ras family GTP-binding proteins H-Ras, Rap1A, and R-Ras with the putative effector molecules Raf kinase and Ral-guanine nucleotide exchange factor. J. Biol. Chem. *271*, 6794–6800.

Hiratsuka, T. (1983). New ribose-modified fluorescent analogs of adenine and guanine nucleotides available as substrates for various enzymes. Biochim Biophys Acta *742*, 496–508.

Huang, L., Hofer, F., Martin, G.S., and Kim, S.-H. (1998). Structural basis for the interaction of Ras with RalGDS. Nat. Struct. Biol. *5*, 422–426.

Jameson, D.M., and Eccleston, J.F. (1997). Fluorescent nucleotide analogs: synthesis and applications. Methods Enzymol. *278*, 363–390.

Jones, T.A., Zou, J.Y., Cowan, S.W., and Kjeldgaard. (1991). Improved methods for building protein models in electron density maps and the location of errors in these models, Acta Crystallogr. A *47*, 110–119.

Kauffmann-Zeh, A., Rodriguez-Viciana, P., Ulrich, E., Gilbert, C., Coffer, P., Downward, J., and Evan, G. (1997). Suppression of c-Myc-induced apoptosis by Ras signalling through PI(3)K and PKB. Nature *385*, 544–548.

Khwaja, A., Rodriguez-Viciana, P., Wennstrom, S., Warne, P.H., and Downward, J. (1997). Matrix adhesion and Ras transformation both activate a phosphoinositide 3-OH kinase and protein kinase B/Akt cellular survival pathway. EMBO J. *16*, 2783–2793.

Kinashi, T., Katagiri, K., Watanabe, S.-I., Vanhaesebroeck, B., Downward, J., and Takatsu, K. (2000). Distinct mechanisms of α5β1 integrin activation by H-Ras and R-Ras. J. Biol. Chem. *275*, 22590–22596.

Kleywegt, G.J. (1999). Experimental assessment of differences between related protein crystal structures. Acta Cryst *D55*, 1878–1884.

Kraulis, P.J. (1991). MOLSCRIPT: A program to produce both detailed and schematic plots of protein structures. J Appl Crystallogr *24*, 946–950.

Krugmann, S., Hawkins, P.T., Pryer, N., and Braselmann, S. (1999). Characterizing the interactions between the two subunits of the p101/p110γ phosphoinositide 3-kinase and their role in the activation of this enzyme by Gβγ subunits. J. Biol. Chem. *274*, 17152–17158.

Leslie, A.G.W. (1992). Recent changes to the MOSFLM package for film and image plate data. In Joint CCP4 and ESF-EACMB Newsletter on Protein Crystallography (Warrington, UK, Daresbury Laboratory).

Lowy, D.R., and Willumsen, B.M. (1993). Function and regulation of Ras. Annu. Rev. Biochem. *62*, 851–891.

Maier, U., Babich, A., and Nurnberg, B. (1999). Roles of non-catalytic subunits in Gβγ-induced activation of class I phosphoinositide 3-kinase isoforms β and γ. J. Biol. Chem. *274*, 29311–29317.

Marshall, C.J. (1996). Ras effectors. Curr. Opin. Cell Biol. *8*, 197–204.

Merritt, E.A., and Bacon, D.J. (1997). Raster3D: Photorealistic Molecular Graphics. Meth Enzymol *277*, 505–524.

Milburn, M.V., Tong, L., deVos, A.M., Brunger, A., Yamaizumi, Z., Nishimura, S., and Kim, S.H. (1990). Molecular switch for signal transduction: structural differences between active and inactive forms of protooncogenic ras proteins. Science *247*, 939–945.

Moodie, S.A., Paris, M., Villafranca, E., Kirshmeier, P., Willumsen, B.M., and Wolfman, A. (1995). Different structural requirements within the switch II region of the Ras protein for interactions with specific downstream targets. Oncogene *11*, 447–454.

Moore, K.J., Webb, M.R., and Eccleston, J.F. (1993). Mechanism of GTP hydrolysis by p21N-ras catalyzed by GAP: studies with a fluorescent GTP analogue. Biochemistry *32*, 7451–7459.

Nassar, N., Horn, G., Herrmann, C., Scherer, A., McCormick, F., and Wittinghofer, A. (1995). The 2.2 A crystal structure of the Ras-binding domain of the serine/threonine kinase c-Raf1 in complex with Rap1A and a GTP analogue. Nature *375*, 554–560.

Nicholls, A., Sharp, K.A., and Honig, B. (1991). Protein folding and association: insights from the interfacial and thermodynamic properties of hydrocarbons. Proteins Struct Funct Genet *11*, 281–296.

Pai, E.F., Kabsch, W., Krengel, U., Holmes, K.C., John, J., and Wittinghofer, A. (1989). Structure of the guanine-nucleotide-binding domain of the Ha-ras oncogene product p21 in the triphosphate conformation. Nature *341*, 209–214.

Pai, E.F., Krengel, U., Petsko, G.A., Goody, R.S., Kabsch, W., and Wittinghofer, A. (1990). Refined crystal structure of the triphosphate conformation of H-ras p21 at 1.35 A resolution: implications for the mechanism of GTP hydrolysis. EMBO J. *9*, 2351–2359.

Rodriguez-Viciana, P., Warne, P.H., Dhand, R., Vanhaesebroeck, B., Gout, I., Fry, M.J., Waterfield, M.D., and Downward, J. (1994).

Phosphatidylinositol-3-OH kinase as a direct target of Ras. Nature *370*, 527–532.

Rodriguez-Viciana, P., Marte, B.M., Warne, P.H., and Downward, J. (1996a). Phosphatidylinositol 3′ kinase: one of the effectors of Ras. Philos Trans R Soc Lond B *351*, 225–232.

Rodriguez-Viciana, P., Warne, P.H., Vanhaesebroeck, B., Waterfield, M.D., and Downward, J. (1996b). Activation of phosphoinositide 3-kinase by interaction with Ras and by point mutation. EMBO J. *15*, 2442–2451.

Rodriguez-Viciana, P., Warne, P.H., Khwaja, A., Marte, B.M., Pappin, D., Das, P., Waterfield, M.D., Ridley, A., and Downward, J. (1997). Role of phosphoinositide 3-OH kinase in cell transformation and control of the actin cytoskeleton by Ras. Cell *89*, 457–467.

Rubio, I., Rodriguez-Viciana, P., Downward, J., and Wetzker, R. (1997). Interaction of Ras with phosphoinositide 3-kinase γ. Biochem. J. *326*, 891–895.

Rubio, I., Wittig, U., Meyer, C., Heinze, R., Kadereit, D., Waldmann, H., Downward, J., and Wetzker, R. (1999). Farnesylation of Ras is important for the interaction with phosphoinositide 3-kinase γ. Eur. J. Biochem. *266*, 70–82.

Runnels, L.W., and Scarlata, S.F. (1998). Regulation of the rate and extent of phospholipase Cβ2 effector activation by the βγ subunits of heterotrimeric G proteins. Biochemistry *37*, 15563–15574.

Scheffzek, K., Ahmadian, M.R., Kabsch, W., Wiesmuller, L., Lautwein, A., Schmitz, F., and Wittinghofer, A. (1997). The Ras-RasGAP complex: Structural basis for GTPase activation and its loss in oncogenic Ras mutants. Science *277*, 333–338.

Shepherd, P.R., Withers, D.J., and Siddle, K. (1998). Phosphoinositide 3-kinase: the key switch mechanism in insulin signalling. Biochem. J. *333*, 471–490.

Shields, J.M., Pruitt, K., McFall, A., Shaub, A., and Der, C.J. (2000). Understanding Ras: 'it ain't over 'til it's over', Trends Cell Biol. *10*, 147–154.

Shioi, T., Kang, P.M., Douglas, P.S., Hampe, J., Yballe, C.M., Lawitts, J., Cantley, L.C., and Izumo, S. (2000). The conserved phosphoinositide 3-kinase pathway determines heart size in mice. EMBO J. *19*, 2537–2548.

Stephens, L.R., Eguinoa, A., Erdjument-Bromage, H., Lui, M., Cooke, F., Coadwell, J., Smrcka, A.S., Thelen, M., Cadwallader, K., Tempst, P., and Hawkins, P.T. (1997). The Gβγ sensitivity of a PI3K is dependent upon a tightly associated adaptor, p101. Cell *89*, 105–114.

Stoyanov, B., Volinia, S., Hanck, T., Rubio, I., Loubtchenkov, M., Malek, D., Stoyanova, S., Vanhaesebroeck, B., Dhand, R., Nurnberg, B., et al. (1995). Cloning and characterization of a G protein-activated human phosphoinositide 3-kinase. Science *269*, 690–693.

Sydor, J.R., Engelhard, M., Wittinghofer, A., Goody, R.S., and Herrmann, C. (1998). Transient kinetic studies on the interaction of Ras and the Ras-binding domain of c-Raf-1 reveal rapid equilibration of the complex. Biochemistry *37*, 14292–14299.

Tanaka, Y., Minami, Y., Mine, S., Hirano, H., Hu, C.D., Fujimoto, H., Fujii, K., Saito, K., Tsukada, J., van Kooyk, Y., et al. (1999). H-Ras signals to cytoskeletal machinery in induction of integrin- mediated adhesion of T cells. J. Immunol. *163*, 6209–6216.

Vanhaesebroeck, B., Welham, M.J., Kotani, K., Stein, R., Warne, P.H., Zvelebil, M.J., Higashi, K., Volinia, S., Downward, J., and Waterfield, M.D. (1997). p110δ, a novel phosphoinositide 3-kinase in leukocytes. Proc Natl Acad Sci U S A *94*, 4330–4335.

Vetter, I.R., Linnemann, T., Wohlgemuth, S., Geyer, M., Kalbitzer, H.R., Herrmann, C., and Wittinghofer, A. (1999). Structural and biochemical analysis of Ras-effector signaling via RalGDS. FEBS Lett. *451*, 175–180.

Walker, E.H., Perisic, O., Ried, C., Stephens, L., and Williams, R.L. (1999). Structural insights into phosphoinositide 3-kinase catalysis and signalling. Nature *402*, 313–320.

Walker, E.H., Pacold, M.E., Perisic, O., Stephens, L., Hawkins, P.T., Wymann, M.P., and Williams, R.L. (2000). Structural determinants of phosphoinositide 3-kinase inhibition by wortmannin, LY294002, quercetin, myricetin, and staurosporine. Mol Cell *6*, 909–919.

White, M.A., Nicolette, C., Minden, A., Polverino, A., Van Aelst, L., Karin, M., and Wigler, M.H. (1995). Multiple Ras functions can contribute to mammalian cell transformation. Cell *80*, 533–541.

Wittinghofer, A., and Herrmann, C. (1995). Ras-effector interactions, the problem of specificity. FEBS Lett. *369*, 52–56.

Wymann, M.P., Sozzani, S., Altruda, F., Mantovani, A., and Hirsch, E. (2000). Lipids on the move: phosphoinositide 3-kinases in leukocyte function. Immunol. Today *21*, 260–264.

Xue, L., Murray, J.H., and Tolkovsky, A.M. (2000). The Ras/phosphatidylinositol 3-kinase and Ras/ERK pathways function as independent survival modules each of which inhibits a distinct apoptotic signaling pathway in sympathetic neurons. J. Biol. Chem. *275*, 8817–8824.

Zhou, J., and Adams, J.A. (1997). Participation of ADP dissociation in the rate-determining step in cAMP- dependent protein kinase. Biochemistry *36*, 15733–15738.

Protein Data Bank ID Code

The coordinates of the Ras·PI3Kγ complex have been deposited in the Protein Data Bank with entry code 1he8.